

# Tuning magnetic exchange interactions in 2D magnets: the case of $\text{CrGeX}_3$ ( $\text{X} = \text{Se}, \text{Te}$ ) and Janus $\text{Cr}_2\text{Ge}_2(\text{Se},\text{Te})_3$ monolayers

Gabriel Martínez-Carracedo<sup>1,2</sup>, Amador García-Fuente<sup>1,2</sup>,

László Oroszlány<sup>3,4</sup>, László Szunyogh<sup>5,6</sup>, and Jaime Ferrer<sup>1,2</sup>

<sup>1</sup>*Departamento de Física, Universidad de Oviedo, 33007 Oviedo, Spain*

<sup>2</sup>*Centro de Investigación en Nanomateriales y Nanotecnología, Universidad de Oviedo-CSIC, 33940, El Entrego, Spain*

<sup>3</sup>*Department of Physics of Complex Systems, Eötvös Loránd University, 1117 Budapest, Hungary*

<sup>4</sup>*Wigner Research Centre for Physics, H-1525, Budapest, Hungary*

<sup>5</sup>*Department of Theoretical Physics, Institute of Physics, Budapest University of Technology and Economics, Műegyetem rkp. 3., H-1111 Budapest, Hungary*

<sup>6</sup>*HUN-REN-BME Condensed Matter Research Group,*

*Budapest University of Technology and Economics,*

*Műegyetem rkp. 3., H-1111 Budapest, Hungary*

We present a computational study to explore the potential of different experimental approaches to tune the magnetic interactions in two-dimensional van der Waals magnets. We selected  $\text{CrGeSe}_3$ ,  $\text{CrGeTe}_3$ , and Janus  $\text{Cr}_2\text{Ge}_2(\text{Se},\text{Te})_3$  monolayers as case studies and calculated the full exchange tensors among all relevant atomic pairs and analyze their dependence on different external parameters, such as biaxial and uniaxial strain, as well as gate voltage. We pay special attention to interactions that emerge or vanish due to changes of the symmetry of the system. We find that biaxial and uniaxial strains significantly modify isotropic exchange couplings, which can lead to a transition from a ferromagnetic to an antiferromagnetic phase, while a gate voltage induces Dzyaloshinskii–Moriya interactions, forming a vortex pattern whose chirality is determined by the sign of the electric field. The electric dipole moment of the Janus material is large, raising the possibility of multiferroic behaviour. The polarizability is similar for the three compounds.

## I. INTRODUCTION

Since the initial experimental report of magnetism in two-dimensional (2D) materials in 2017 [1, 2], the interest of the scientific community in van der Waals (vdW) magnets has greatly increased. On the one hand, they promise to be strong candidates for future magnetic memory technologies like MRAM-based devices [3, 4] and due to their layered exfoliation behavior they can successfully facilitate the miniaturization process. On the other hand, the magnetic domain structure found in 2D vdW magnets [5, 6] might open the way toward developing domain wall memory technology in 2D materials [7]. Long-range magnetic order appears in 2D vdW magnets because the magnetic anisotropies arising from spin-orbit coupling (SOC) are large enough to overcome thermal and quantum fluctuations [8]. However, the experimental Curie temperatures ( $T_c$ ) of these materials remain relatively low: 35 K for  $\text{CrI}_3$  monolayer [1] or 175 K for 10 layer thick  $\text{Fe}_3\text{GeTe}_2$  [9]. More promisingly, SOC can lead to non-collinear magnetic configurations, such as helical states [10, 11] or spin textures [12, 13] that have been suggested to be candidates for data storage [14]. In most cases these are caused by the antisymmetric exchange, i.e., the Dzyaloshinskii–Moriya (DM) interaction. In centrosymmetric materials like  $\text{NiI}_2$  monolayers, where the DM interaction vanishes because of inversion symmetry, skyrmionic structures can be stabilized with the aid of symmetric exchange [15].

The recently developed computational tool GROGU [16] enables us to quantify the bilinear tensorial exchange

interactions between any two atomic magnetic entities from first principles calculations, well beyond the capability of methods based on energy differences [17]. In this work, we take advantage of this tool to analyze how different parameters, which can be controlled experimentally, affect these interactions and could even lead to a change in the magnetic configuration of a 2D vdW magnet. In particular, we consider two types of effects. One is the change in the bond distances and angles between magnetic atoms, which can be controlled by the application of strain. As we show here, strain can have a strong effect on the magnitude and even the sign of the magnetic interactions, eventually inducing a phase transition between ferromagnetic (FM) and antiferromagnetic (AFM) states. A second approach consists of changing the system’s symmetry, which can be achieved by atomic changes in the structure, uniaxial strain, or the application of a gate voltage. Certain magnetic interactions are forbidden in high-symmetry structures, while lowering the symmetry of the system can allow some of those interactions to appear. We show that large DM interactions can be activated and tuned by uniaxial strain, and especially by a gate voltage. Such effects then can promote the appearance of non-collinear magnetic structures with a simple experimental knob. In fact, experiments proved that a gate voltage can tune the chirality of skyrmions in centrosymmetric monolayers such as  $\text{CrGeTe}_3$  (CGT) [18].

To illustrate how magnetic transitions can be triggered, we study the monolayers of  $\text{CrGeSe}_3$  (CGS) and  $\text{CrGeTe}_3$  (CGT). The magnetic, electronic, and

magnonic properties of these vdW materials have been widely studied [19–23], and interest in them has increased in part because of the new 2D physics they can offer. CGS and CGT monolayers possess a rhombohedral structure and are characterized by the space group  $R\bar{3}$ . Their minimal unit cell contains 10 atoms and the structure is depicted in Fig. 1(a). We also study a Janus version of this structure, where the top external layer is formed by Te and the bottom external by Se atoms as depicted in Fig. 1(b). This system corresponds to the  $\text{Cr}_2\text{Ge}_2(\text{Se},\text{Te})_3$  (CGST) stoichiometry. Phonon spectra calculations have shown that these lattice structures are stable [24]. Recently, Monte-Carlo calculations have shown that Janus CGST can stabilize skyrmionic states [24]. Other Janus magnets that have been studied in the past are  $\text{Cr}_2(\text{I},\text{X})_3$  ( $\text{X} = \text{Br}, \text{Cl}, \text{F}$ ) [25, 26],  $\text{Ni}(\text{X},\text{Y})$  ( $\text{X}, \text{Y} = \text{I}, \text{Br}, \text{Cl}$ ) [27] or  $\text{Cr}(\text{Y},\text{X})$  ( $\text{Y} = \text{S}, \text{Se}, \text{Te}; \text{X} = \text{Cl}, \text{Br}, \text{I}$ ) [28]. The interest in Janus magnets lies in the fact that due to the lack of inversion symmetry it is easier to induce non-collinear magnetic textures triggered by non-zero DM interactions [24], providing a solid platform for skyrmion-based devices in the near future.

In section II we define the parts of the spin Hamiltonian used to model the magnetic interactions and determine which ones vanish due to the symmetry of the systems under consideration. In section III we give the details of the calculations. In section IV we present and explain the results obtained when biaxial and uniaxial strain, as well as a gate voltage are applied. Finally, in Section V we summarize and draw our conclusions.

## II. SPIN MODEL AND SYMMETRY CONSTRAINTS

Most magnetic materials with localized magnetic moments can be described by the classical Heisenberg Hamiltonian:

$$H(\{\mathbf{e}_i\}) = \frac{1}{2} \sum_{i \neq j} \mathbf{e}_i \mathcal{J}_{ij} \mathbf{e}_j + \sum_i \mathbf{e}_i \mathcal{K}_i \mathbf{e}_i, \quad (1)$$

where  $\mathbf{e}_i$  is a unit vector pointing along the spin-only magnetic momentum of the magnetic atom located on site  $i$ ,  $\mathcal{K}_i$  is the on-site anisotropy matrix on site  $i$ , and  $\mathcal{J}_{ij}$  is the exchange tensor that can be written as the sum of a symmetric and an antisymmetric part:

$$\begin{aligned} \mathcal{J}_{ij} &= \mathcal{J}_{ij}^s + \mathcal{J}_{ij}^a = \\ &= \begin{pmatrix} J_{ij}^{xx} & S_{ij}^z & S_{ij}^y \\ S_{ij}^z & J_{ij}^{yy} & S_{ij}^x \\ S_{ij}^y & S_{ij}^x & J_{ij}^{zz} \end{pmatrix} + \begin{pmatrix} 0 & D_{ij}^z & -D_{ij}^y \\ -D_{ij}^z & 0 & D_{ij}^x \\ D_{ij}^y & -D_{ij}^x & 0 \end{pmatrix}. \end{aligned} \quad (2)$$

The DM vectors are then defined as  $\mathbf{D}_{ij} = (D_{ij}^x, D_{ij}^y, D_{ij}^z)$ . It is common to write the spin-

Hamiltonian (1) in the following form,

$$\begin{aligned} H(\{\mathbf{e}_i\}) &= \frac{1}{2} \sum_{i \neq j} J_{ij}^H \mathbf{e}_i \cdot \mathbf{e}_j + \frac{1}{2} \sum_{i \neq j} \mathbf{e}_i \mathcal{J}_{ij}^S \mathbf{e}_j + \\ &+ \frac{1}{2} \sum_{i \neq j} \mathbf{D}_{ij} \cdot (\mathbf{e}_i \times \mathbf{e}_j) + \sum_i \mathbf{e}_i \mathcal{K}_i \mathbf{e}_i, \end{aligned} \quad (3)$$

where  $J_{ij}^H = \frac{1}{3} \text{Tr} J_{ij}^s$  is the isotropic Heisenberg coupling and  $\mathcal{J}_{ij}^S = \mathcal{J}_{ij}^s - J_{ij}^H \mathcal{I}$  is a traceless symmetric matrix.

The knowledge of the exchange constants is crucial for computing and predicting the order-disorder transition temperature  $T_c$ , the magnon spectra or the spin pair correlation functions. Moreover, external control over these constants through electric fields or strain can result in magnetic phase transitions [29–32], generate skyrmionic textures [33, 34] or tune  $T_c$  [35].

In our calculations,  $\mathcal{J}_{ij}$  is computed at the local frame of reference shown in Fig. 2(a), while the corresponding atomic pairs  $ij$  are labeled as indicated in Fig. 1(b). In this figure, each pair  $ij \in \{c1, c2, c3, c4\}$  exhibits a different point group symmetry, that leads to different selection rules for the exchange constants. In the Appendix, we summarize the selection rules for the exchange constants when inversion symmetry ( $\Pi$ ), mirror  $\alpha\beta$ -plane symmetry ( $\sigma_{\alpha\beta}$ ), and  $C_2$  symmetry around the  $\alpha$ -axis ( $C_{2\alpha}$ ) (where  $\alpha, \beta = x, y$ , and  $z$ ) are present with respect to the center of a given bond. We apply these rules to identify the non-zero exchange parameters and the corresponding symmetries for the CGS and CGST structures, see Table I. The Janus structure of CGST breaks  $\Pi$ ,  $\sigma_{xy}$ ,  $C_{2x}$  and  $C_{2y}$  symmetries that are present in CGS and CGT. For CGST, the first and third neighbors have non-zero  $D^y$  and  $D^z$  values, which vanish for CGS and CGT. We will demonstrate that it is also possible to induce  $D^y$  in CGS and CGT between first neighbors by a gate voltage that breaks inversion symmetry. In Fig. 2(b-d) we show a sketch of how different DM vector components induce non-collinear magnetic configurations.

## III. COMPUTATIONAL METHOD

We compute all terms in the spin-Hamiltonian given in Eq. (3) by a two-step process. First, we obtain the electronic Hamiltonian based on the Density Functional Theory (DFT) [36, 37] by using the SIESTA code [38]. This code has the advantage that electronic wave functions are expanded in a basis of pseudo-atomic orbitals, from which it is easy to identify the atomic magnetic moments. In a second step, the DFT Hamiltonian is used as input of the package GROGU [16], which extracts the exchange and anisotropy constants of the system based on the magnetic force theorem [39, 40].

Our DFT calculations employed the Generalized Gradient Approximation (GGA) in the scheme of Perdew-Burke-Ernzerhof (PBE) [41] for the exchange-correlation potential. A  $10 \times 10 \times 1$  Monkhorst-Pack  $k$ -point grid and

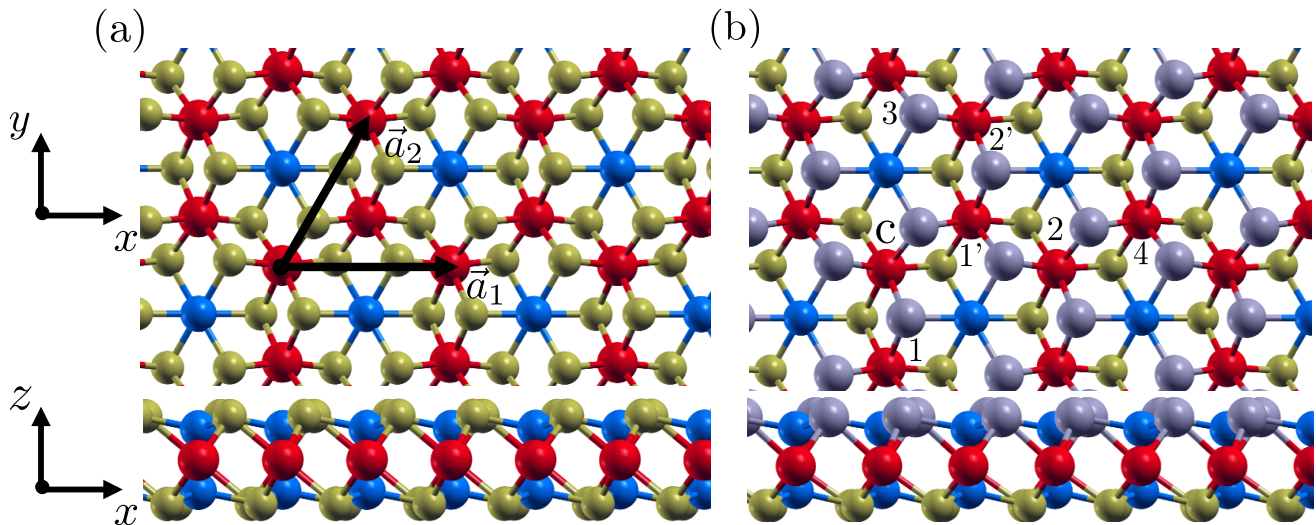


FIG. 1. Top and side views of (a) the CGS and (b) the Janus CGST structures. Cr, Ge, Se and Te atoms are depicted in red, blue, yellow and grey, respectively. Lattice vectors  $\vec{a}_1$  and  $\vec{a}_2$  are shown in (a). Labeling of the nearest Cr neighbors with respect to a reference atom  $c$  is also shown in (b).

TABLE I. Symmetries and non-zero exchange parameters for the four nearest neighbors in CGS / CGST structures following the local frame of reference depicted in Fig 2(a). For simplicity, we removed  $J^{xx}$ ,  $J^{yy}$  and  $J^{zz}$  from the list of non-zero exchange parameters as there are no selection rules for these matrix elements.

Bond	Symmetries centered on $C$	Non-zero exchange parameters
c1	$\Pi, \sigma_{yz}, C_{2y} / \sigma_{yz}$	$S^x / D^y, D^z, S^x$
c2	$C_{2y} / \emptyset$	$D^x, D^z, S^y / D^x, D^y, D^z, S^x, S^y, S^z$
c3	$\Pi, \sigma_{yz}, C_{2y} / \sigma_{yz}$	$S^x / D^y, D^z, S^x$
c4	$\Pi / \emptyset$	$S^x, S^y, S^z / D^x, D^y, D^z, S^x, S^y, S^z$

a mesh cut-off of 1000 Ry for reciprocal / real-space integrals were used for an accurate self-consistent convergence. We employed a double- $\zeta$  polarized basis set whose first- $\zeta$  PAOs had long radii of about 8 Bohr. All calculations were carried out using structural relaxations with a maximum force tolerance equal to 0.005 eV/Å. Interactions with the core electrons were included by a Troullier-Martins pseudopotential [42], obtained as described in Ref. [43]. For the GROGU calculations, a  $100 \times 100 \times 1$  Monkhorst-Pack  $k$ -grid was used and localized magnetic moments were projected onto the Cr  $3d$ -orbitals to avoid undesired contributions from non-magnetic orbitals [16].

#### IV. RESULTS

First, we obtained the structural and electronic ground state of the three systems, CGS, CGT and CGST. A summary of the results is given in Table II. The lattice constant of CGST lies in between those of CGS and CGT, as expected. As of the magnetic structure, all these systems are ferromagnetic with a similar magnetic moment localized on each Cr atom, while all other atoms are non-magnetic. The orbital contribution to the magnetic moments is below 1 % in all cases. We define the magnetic anisotropy energy (MAE) as the difference of

the self-consistently calculated total energy between in-plane and out-of-plane magnetizations,  $MAE = E_{\parallel} - E_{\perp}$ . The MAE shows a preference of in-plane magnetization for CGS, while CGT and CGST present an out-of-plane easy axis. This is consistent with experimental reports for CGT [2]. All compounds are semiconducting, with a band gap well below 1 eV.

TABLE II. Summary of the structural, electronic and magnetic properties of CGS, CGT and CGST from the SIESTA calculations.

	CGS	CGT	CGST
Lattice constant (Å)	6.44	6.98	6.71
Spin moment ( $\mu_B$ )	3.531	3.749	3.643
Orbital moment ( $\mu_B$ )	0.017	0.035	0.025
MAE (meV/Cr)	-0.05	0.80	0.15
Band gap (eV)	0.7	0.2	0.3

Next we computed the exchange parameters for these compounds up to the fourth nearest neighbor, and summarized our results in Table III. The interactions are given in the local frame of reference shown in Fig. 2(a), while the corresponding pairs of atoms  $ij$  are labeled as depicted in Fig. 1(b). The negative value of  $J_{c1}^H$  indicates that the interaction between first neighbors is FM, which agrees well with experimental results for CGT [1]

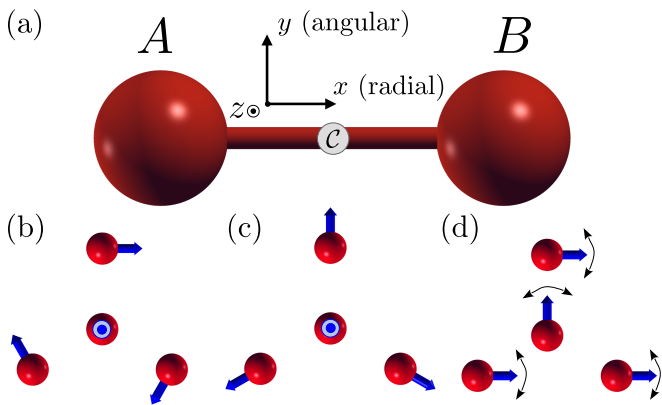


FIG. 2. (a) Schematic picture of the local frame of reference, where the bond connecting the A and B atoms is parallel to the  $x$ -axis. The positive  $z$  direction points towards the reader. Symmetries and selection rules are computed with respect to the center  $C$ . (b-d) Sketch of non-collinear textures induced by DM vectors at first nearest neighbors relative to the central atom. Magnetic moments are represented by blue arrows. (b) A vortex pattern is formed around the central atom if only a radial DM component is present. (c) A radial vortex pattern is formed around the central atom if only an angular DM component is present. In panels (b) and (c), the spin in the central atom is pointing towards the reader. (d) An in-plane relative  $90^\circ$ -degree orientation among first neighbors is boosted when the nearest neighbor DM vectors are normal to the  $xy$  plane. The thin curved arrows demonstrate that this magnetic pattern can be rotated in the plane at zero energy cost.

and other theoretical results [21, 24]. The uniaxial on-site anisotropy energy,  $K_c^{xx} - K_c^{zz}$ , is approximately  $\sim 15$  times larger in CGT than in CGS and 3 times larger than in CGST. This highlights the effect of SOC interaction in heavy atoms such as Te compared to the lighter atoms like Se. On-site anisotropy values for these materials show a preference of in-plane magnetization. However, the two-site exchange anisotropy  $J_{cj}^{xx} - J_{cj}^{zz}$  and  $J_{cj}^{yy} - J_{cj}^{zz}$ , also contributes to the total MAE, especially at first neighbors ( $j = 1$ ). We find that it is this type of magnetic anisotropy that leads to out-of-plane magnetization in CGT and CGST.

The only off-diagonal component of the symmetric exchange tensor that doesn't vanish by symmetry is  $S_{c1}^x$ , but its value is very small as compared to the isotropic interactions, with no relevant differences among the three structures. Conversely, DM vectors at first nearest neighbors appear only for the Janus CGST compound due to the breaking of inversion symmetry. Of particular interest is the DM vector component  $D_{c1}^y$  for CGST, with a value that is approximately  $\sim 16\%$  of the isotropic exchange  $J_{c1}^H$  and agrees well with VASP supercell calculations [24]. Remarkably, this component could induce the formation of radial vortex magnetic patterns in CGST as shown in Fig. 2(c).

TABLE III. Exchange parameters for CGS, CGT and CGST in the local reference frame given by Fig. 2(a). All quantities are given in meV units. Atomic labels correspond to those defined in Fig. 1 (b). Due to  $C_3$  symmetry  $K_c^{xx} = K_c^{yy}$ . The values for  $S_{c2}^\alpha$  are omitted in the table since their magnitudes are below 0.01 meV, with the exception of  $S_{c2}^x$  in CGST where it is 0.04 meV.

	CGS	CGT	CGST
$K_c^{xx} - K_c^{zz}$	-0.03	-0.47	-0.15
$J_{c1}^H$	-0.86	-7.04	-4.38
$J_{c1}^{xx} - J_{c1}^{zz}$	-0.01	-0.06	0.03
$J_{c1}^{yy} - J_{c1}^{zz}$	0.09	0.72	0.58
$S_{c1}^x$	-0.01	-0.02	-0.04
$D_{c1}^y$	-	-	0.70
$D_{c1}^z$	-	-	-0.19
$J_{c2}^H$	0.28	0.19	0.72
$J_{c2}^{xx} - J_{c2}^{zz}$	<0.01	-0.02	-0.04
$J_{c2}^{yy} - J_{c2}^{zz}$	-0.01	-0.05	-0.04
$D_{c2}^x$	-0.16	-0.19	-0.16
$D_{c2}^y$	-	-	0.07
$D_{c2}^z$	-0.19	-0.42	-0.25
$J_{c3}^H$	0.30	-0.25	0.24
$J_{c3}^{xx} - J_{c3}^{zz}$	<0.01	-0.11	-0.12
$J_{c3}^{yy} - J_{c3}^{zz}$	-0.02	0.04	-0.05
$S_{c3}^x$	-0.02	-0.14	-0.10
$D_{c3}^y$	-	-	-0.02
$D_{c3}^z$	-	-	-0.28
$J_{c4}^H$	0.21	0.19	0.24

### A. Biaxial Strain

After describing the magnetic interactions in the ground state, we focus on different effects that could be applied experimentally to modify these interactions, eventually triggering a controllable change in the magnetic response of those systems. We consider first the effect of homogeneous biaxial strain. This is simulated by relaxing the structures for different fixed in-plane lattice constants. With respect to the ground state geometry, we look for strains in the range of  $\pm 4\%$ . In this range, the easy axis for the three materials remains unchanged, and the magnetic moments vary by approximately 2%, ensuring that the ground state multiplet is not affected by the strain.

Biaxial strain does not affect the symmetry of the system. As a consequence, we find that the most relevant changes happen in the isotropic exchange constants. These are plotted in Fig. 3 as a function of strain. The first neighbor interactions are the most sensitive on the strain because of the Goodenough-Kanamori-Anderson (GKA) mechanism [44–46]. This phenomenon is related to the angle formed by consecutive Cr-X-Cr bonds (X = Se or Te), that increases with strain. When the angle passes the critical value of  $\sim 90^\circ$  an AFM/FM transition takes place. This mechanism explains that at short Cr-Cr distances the interaction at first nearest neighbors is AFM, but when the distance increases, a FM superexchange interaction mediated by Te or Se takes over. The

same mechanism is found in other magnetic systems such as 1T-CrTe<sub>2</sub> [47], CrSiTe<sub>3</sub> [48] or other Janus magnets like Cr<sub>2</sub>(X,Y)Te<sub>6</sub> (X, Y = Ge, Si, Sn) [49].

The isotropic Heisenberg interactions for CGS are shown in Fig. 3(a) as a function of the lattice constant. For this compound, a compression of only  $\sim 0.35\%$  changes the sign of  $J_{1c}^H$  to favor AFM interaction. Moreover, a larger compression of the order of  $\sim 3\%$  results in  $J_{c1}^H \sim 8$  meV, which is about four times larger than the second strongest isotropic coupling. This implies that CGS is a 2D magnet, where the ground state can be switched from FM to AFM experimentally through feasible biaxial compression.

As clear from Figs. 3(b) and (c), for the other two compounds larger compressions,  $\sim 2.7\%$  for CGT and  $\sim 1.6\%$  for CGST, are needed to have a sign change in  $J_{c1}^H$ . In case of a few strain values, in Table IV we listed the angles between the Cr-Se/Te and Se/Te-Cr bonds connecting nearest neighbor Cr atoms. Regarding  $J_{c1}^H$  for these strain values we find a good agreement with the GKA mechanism. Note that for lattice constants below the FM-AFM transition for  $J_{c1}^H$ , all isotropic constants up to the fourth nearest neighbors become positive (AFM coupling), indicating the loss of FM collinear magnetic order.

Beyond the effect on the isotropic exchange constants, we also noticed significant impacts of biaxial strain on the DM vectors, in particular, for  $\mathbf{D}_{c2}$ . In the considered range of strain,  $D_{c2}^x$  varies between about -0.1 and -0.2 meV in CGT, while  $D_{c2}^z$  varies between -0.1 and -0.2 meV in CGS and between -0.3 and -0.4 meV in CGT.

TABLE IV. Angle subtended for the bonds Cr-X-Cr (X=Te and Se) in the three materials for some values of the biaxial strain. For CGST it is shown the bond angles for Cr-Te-Cr / Cr-Se-Cr.

Biaxial Strain	CGS	CGT	CGST
-3%	87.61°	88.63°	84.33° / 91.52°
0%	89.94°	90.97°	86.98° / 94.05°
+3%	92.11°	93.12°	87.72° / 94.70°

## B. Uniaxial Strain

Next we investigate the effect of uniaxial strain on the exchange interactions. We simulate a strain in the range of  $\pm 5\%$  applied only over the direction of  $\vec{a}_1$ , as defined in Fig. 1(a). This strain breaks  $C_3$  symmetry, therefore, the  $c1$  and  $c1'$  bonds are no longer equivalent. This implies the lifting of degeneracy between the isotropic exchange parameters  $J_{c1}^H$  and  $J_{c1'}^H$ , which can have different characteristics depending on the distance between Cr atoms and, consequently, on the Cr-X-Cr (X = Te, Se) bond angles. The difference between the angles subtended by the  $c1$  and  $c1'$  types of Cr-X-Cr bonds,  $\Delta\alpha$ , is shown in Table. V. The values of  $\Delta\alpha$  are of the order of the differences between the angles shown in Table IV,

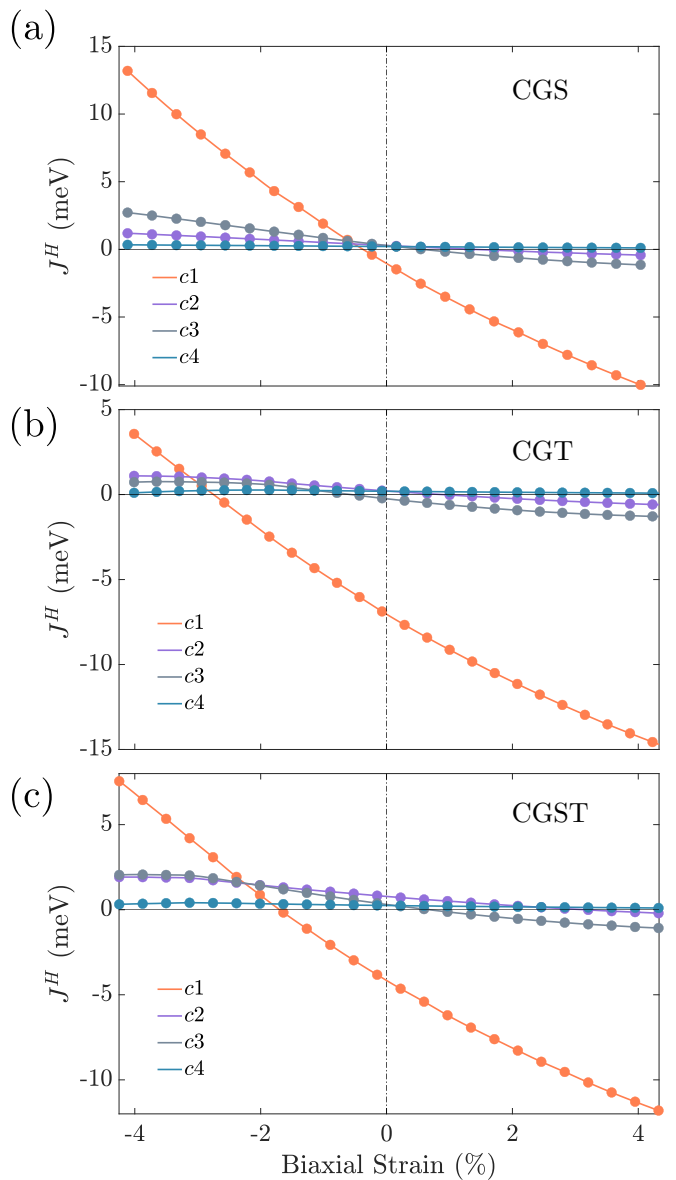


FIG. 3. Isotropic exchange constants up to the fourth nearest neighbors as a function of the biaxial strain for (a) CGS, (b) CGT and (c) CGST. The labels  $c_j$  ( $j = 1, 2, 3$  and 4) refer to pairs of sites as depicted in Fig. 1(b).

indicating that the effect of the GKA mechanism might be very different for the  $c1$  and  $c1'$  bonds.

TABLE V. Difference  $\Delta\alpha$  between the angles subtended by the Cr-X-Cr bonds along the  $c1$  and  $c1'$  nearest neighbors, when  $\pm 3\%$  uniaxial strain is applied over the  $\vec{a}_1$  direction. For CGST,  $\Delta\alpha$  is presented for the Cr-Te-Cr / Cr-Se-Cr bonds.

Uniaxial Strain	CGS	CGT	CGST
-3%	2.30°	2.42°	2.18° / 2.48°
+3%	-2.33°	-2.45°	-2.22° / -2.31°

In Fig. 4 the non-equivalent isotropic couplings for the nearest neighbors are shown as a function of the uniaxial

strain. All the  $J_{c1}^H$  curves present similar slopes, considerably larger than those of  $J_{c1'}^H$ . This is a consequence of the  $c1$  bond located in the direction of the strain, and therefore being more sensitive to its magnitude. Due to these different slopes, we find regions of compressive strain where  $J_{c1}^H$  changes sign to AFM coupling but  $J_{c1'}^H$  remains FM. Most likely, these strain values would favor a magnetic structure of FM coupled rows of Cr atoms in direction perpendicular to the strain, with AFM coupling between rows. The needed compression to obtain this transition is of only  $\sim 1\%$  for CGS, while a larger value of  $\sim 3\%$  ( $\sim 5\%$ ) is needed for CGST (CGT).

Focusing on the impact of uniaxial strain on the DM vectors we can note that most bonds retain their symmetries under uniaxial strain. The most obvious exception is  $c2'$ , since upon uniaxial strain the distance from site  $1'$  to  $c$  will differ from that between sites  $1'$  to  $2'$ , and the  $C_{2y}$  symmetry in the local frame of reference, see Fig. 2(a) and Table I, gets broken. This does not happen for the  $c2$  bond however. Therefore,  $D_{c2}^y$  is induced by uniaxial strain. The magnitude of  $D_{c2}^y$ , induced by  $\pm 5\%$  uniaxial strain is  $\mp 0.1$  meV ( $\mp 0.05$  meV) that is  $\sim 50\%$  ( $16\%$ ) of  $J_{c2}^H$ , for CGT (CGS). Recall that  $C_{2y}$  symmetry was already broken in CGST and  $D_{c2}^y$  is different from zero even when uniaxial strain is not applied. No other relevant changes are observed for the relativistic exchange parameters, apart from those observed for biaxial strain.

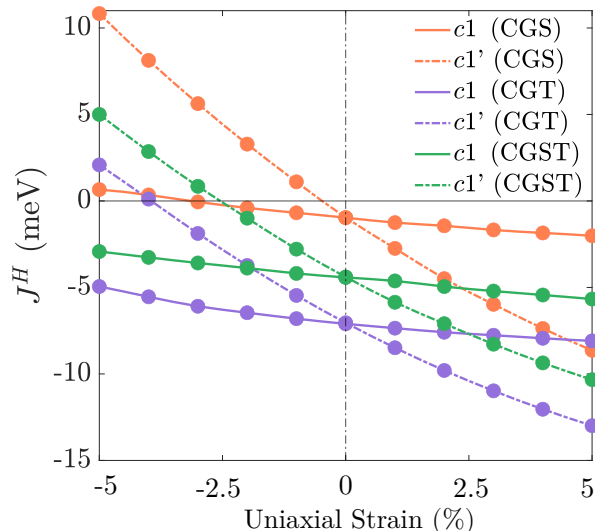


FIG. 4. Nearest neighbor isotropic exchange couplings as a function of uniaxial strain over  $\bar{a}_1$  for CGS (orange), CGT (purple) and CGTS (green). The interactions for the pairs split by the strain, labeled by  $c1$  and  $c1'$ , show remarkably different dependence on the strain. The labels  $cj$  ( $j = 1$  and  $1'$ ) refer to nearest neighbor pairs of sites as depicted in Fig. 1(b).

### C. Gate voltage

We simulate the effect of gate voltage by including in our simulations an electric field  $\mathcal{E}_z$  perpendicular to the monolayer. The main effect of such an electric field is breaking the inversion symmetry of the CGS and CGT structures which induces DM interactions in the system [18, 50–53], while the isotropic and other exchange parameters are hardly affected by the gate voltage. We find that  $\mathcal{E}_z$  produces a linear response in  $D_{c1}^y$  for CGS and CGT which was zero in the absence of the field. Inversion symmetry is already broken for CGST without electric field, however, a change in the magnitude of the DM vectors proportional to the electric field is also observed. Fig. 5(a) indicates that in CGS and CGT the chirality of the first nearest neighbor DM vectors, each parallel to the local  $y$  axis, is controlled by the sign of the electric field. In case of CGST, we find that  $D_{c1}^y > 0$ , so the chirality of the DM vectors is the one shown in the right picture in Fig. 5(a) in the investigated range of the electric field.

Fig. 5(b) demonstrates the linear response in  $D_{c1}^y$  to the applied electric field for the three materials. A linear fit  $\Delta D_{c1}^y(\mathcal{E}_z) = \mathcal{P}_X \cdot \mathcal{E}_z$  shows that  $\mathcal{P}_{\text{CGS}} = -0.11$  e $\cdot\text{\AA}$ ,  $\mathcal{P}_{\text{CGT}} = -0.36$  e $\cdot\text{\AA}$  and  $\mathcal{P}_{\text{CGST}} = -0.10$  e $\cdot\text{\AA}$ . The induced  $D_{c1}^y$  component can achieve 3% and 1.6% of  $J_{c1}^H$  with  $\mathcal{E}_z = 0.3$  V/ $\text{\AA}$  for CGS and CGT, respectively. For CGST, the linear response is small compared to the value in the absence of the field, and this induces a total magnitude change of 6% of  $D_{c1}^y(\mathcal{E}_z = 0)$ . Remarkably, in this compound  $D_{c1}^y$  is between 15-16% of  $J_{c1}^H$  for  $\mathcal{E}_z \in [-0.3, 0.3]$  V/ $\text{\AA}$ .

The electrically induced DM interaction  $D_{c1}^y$  is further enhanced by biaxial strain. We found that a strain of 3% increases the magnitude of  $D_{c1}^y$  by  $\sim 60\%$  when  $\mathcal{E}_z = 0.3$  V/ $\text{\AA}$  is applied for CGS and CGT. Moreover, a biaxial compression of 3% reduces the magnitude of  $D_{c1}^y$  by 30% and 46% for CGS and CGT, respectively.

Lastly, we comment on the potential ferroelectric properties that can be found in Janus magnets [25, 54–56] like CGST. We find that the total electric dipole moment of CGS, CGT and CGST per unit cell follows the linear response relationship

$$\mathcal{P}_T = \mathcal{P}_0 + \alpha \mathcal{E}_z \quad (4)$$

where  $\alpha$  is the material's polarizability, see Fig. 6. We find that the  $z$ -axis charge asymmetry in CGST produces a non-zero  $\mathcal{P}_0 = 0.16$  e $\cdot\text{\AA}$ . The obtained  $\mathcal{P}_0$  in this Janus magnet is about ten times larger than those obtained through bilayer stacking engineering [57, 58]. The simultaneous presence of the electric dipole moment and magnetization in the same phase confirms the multiferroic behavior of CGST. Furthermore, a negative electric field larger in magnitude than  $\mathcal{E}_z = 0.1$  V/ $\text{\AA}$  reverses the sign of  $\mathcal{P}_T$ , as shown in Fig. 6. For CGS and CGT,  $\mathcal{P}_0$  is zero. We find that the polarizability is similar for the three compounds. The proportionality of  $D_{c1}^y$  with the

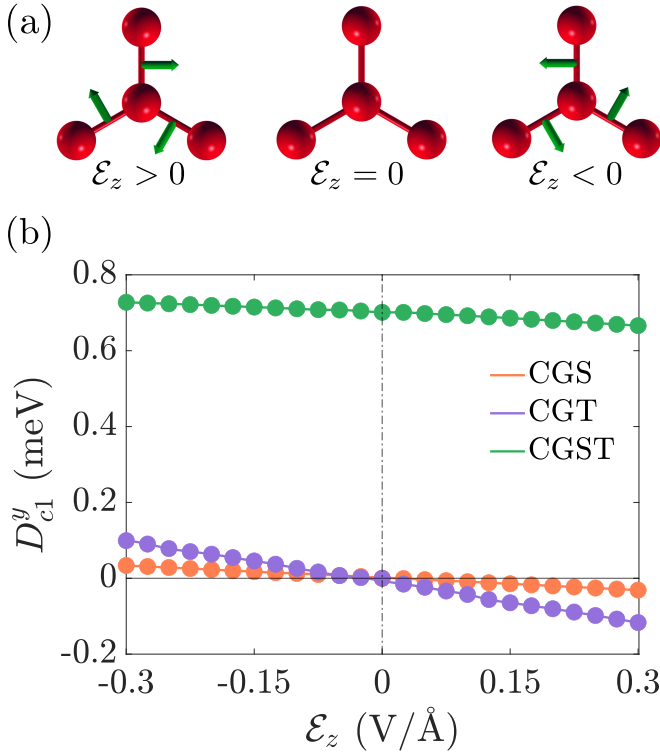


FIG. 5. (a) Schematic drawing of the angular vortex pattern of the nearest neighbor DM vectors depending on the sign of the applied electric field normal to a monolayer of CGS and CGT. (b)  $D_{c1}^y$  as a function of the electric field for CGS (orange), CGT (purple) and CGST (green). CGS and CGT curves cross the origin because of the inversion symmetry of the system when  $\mathcal{E}_z = 0$ , unlike in the case of CGST.

electric field seen in Fig. 5(b) is consistent with the linear response  $\mathcal{P}_T \propto \mathcal{E}_z$  [51, 59].

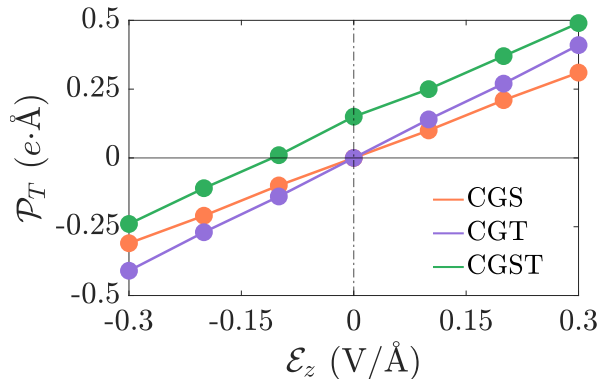


FIG. 6. Total electric dipole moment  $\mathcal{P}_T$  measured in  $e \cdot \text{Å}$  along the  $z$ -axis for the three different materials. In absence of electric field, CGST has a total dipole equal to  $0.15 e \cdot \text{Å}$  that can be switched with electric fields below  $-0.1 \text{ V}/\text{Å}$ .

## V. SUMMARY AND CONCLUSIONS

We presented a computational study of the impact of symmetry breaking induced by different experimental approaches on the magnetic properties of 2D vdW materials. We calculated the tensorial exchange parameters for  $\text{CrGeS}_3$ ,  $\text{CrGeTe}_3$ , and  $\text{Cr}_2\text{Ge}_2(\text{Se},\text{Te})_3$  using the program package GROGU [16] based on the relativistic version [40] of the LKAG formalism [39]. CGST exhibits ferroelectric properties and is a candidate to support magnetic textures due to DM interaction arising from the lack of inversion symmetry [24]. Biaxial strain can trigger a FM/AFM transition among first neighbors with experimentally feasible compressions of approximately 0.4, 2, and 3% for CGS, CGST, and CGT, respectively. Uniaxial strain produces a difference between isotropic couplings for the  $c1$  and  $c1'$  types of nearest neighbor bonds, and reasonable values of compression (1%, 3% and 5% for CGS, CGST and CGT, respectively) results to isotropic couplings  $J_{c1}^H > 0$  and  $J_{c1}^H < 0$ . These couplings then promote a row-wise AFM texture of the Cr spins observed in other monolayer systems [60, 61]. Uniaxial strain breaks  $C_{2y}$  symmetry along the next nearest neighbor  $c2'$  bond and induces  $D_{c2}^y$ , component that can achieve 50%/16% of  $J_{c2}^H$  for CGT/CGS. A gate voltage perpendicular to the monolayer breaks inversion symmetry for CGS and CGT, and  $D_{c1}^y$  emerges in linear response to the electric field, forming a vortex pattern at the first nearest neighbors whose chirality is tuned by the sign of the electric field. Our computational results clearly demonstrate that relevant exchange parameters for the 2D vdW ferromagnets CGS, CGT, and CGST can be tuned by feasible external control to achieve magnetic phase transitions.

## ACKNOWLEDGEMENTS

G. M.-C., A. G.-F. and J. F. have been funded by Ministerio de Ciencia, Innovación y Universidades, Agencia Estatal de Investigación, Fondo Europeo de Desarrollo Regional via the grants PGC2018-094783 and PID2022-137078NB-I00, and by Asturias FICYT under grant AYUD/2021/51185 with the support of FEDER funds. G. M.-C. has been supported by Programa “Severo Ochoa” de Ayudas para la investigación y docencia del Principado de Asturias. This work was supported by the Ministry of Culture and Innovation and the National Research, Development and Innovation Office within the Quantum Information National Laboratory of Hungary (Grant No. 2022-2.1.1-NL-2022-00004) and projects K131938, K142179. We thank the “Frontline” Research Excellence Programme of the NRDIO, Grant No. KKP133827. This project has received funding from the HUN-REN Hungarian Research Network.

## APPENDIX: SYMMETRY CONSIDERATIONS

Here we summarize the selection rules that occur over the exchange constants of the Heisenberg Hamiltonian in Eq. (2) due to the invariance of the structure under certain symmetry operations. These rules are the extension of Moriya's rules for the DM vectors [62]. The symmetry operations are performed with origin at the center  $\mathcal{C}$  of the bond between the atoms  $A$  and  $B$ , as previously shown in Fig. 2(a). The rules are the following:

1. Inversion symmetry ( $\Pi$ ) respect to  $\mathcal{C}$ :  
 $D_{AB}^x = D_{AB}^y = D_{AB}^z = 0$ .

2.  $yz$ -plane symmetry ( $\sigma_{yz}$ ) passing through  $\mathcal{C}$ :  
 $S_{AB}^y = S_{AB}^z = D_{AB}^x = 0$ .

3.  $xz$ -plane symmetry ( $\sigma_{zx}$ ) passing through  $\mathcal{C}$ :  
 $S_{AB}^x = S_{AB}^z = D_{AB}^x = D_{AB}^z = 0$ .

4.  $xy$ -plane symmetry ( $\sigma_{xy}$ ) passing through  $\mathcal{C}$ :  
 $S_{AB}^x = S_{AB}^y = D_{AB}^x = D_{AB}^y = 0$ .

5.  $C_2$  symmetry along  $z$ -axis ( $C_{2z}$ ) passing through  $\mathcal{C}$ :  
 $S_{AB}^x = S_{AB}^y = D_{AB}^z = 0$ .

6.  $C_2$  symmetry along  $y$ -axis ( $C_{2y}$ ) passing through  $\mathcal{C}$ :  
 $S_{AB}^x = S_{AB}^z = D_{AB}^y = 0$ .

7.  $C_2$  symmetry along  $x$ -axis ( $C_{2x}$ ) passing through  $\mathcal{C}$ :  
 $S_{AB}^y = S_{AB}^z = D_{AB}^y = D_{AB}^z = 0$ .

8.  $C_n$  ( $n > 2$ ) symmetry along  $x$ -axis ( $C_{nx}$ ) passing through  $\mathcal{C}$ :  
 $S_{AB}^x = S_{AB}^y = S_{AB}^z = D_{AB}^y = D_{AB}^z = 0$  and  $J_{AB}^{xx} = J_{AB}^{yy}$ .

- 
- [1] B. Huang, G. Clark, E. Navarro-Moratalla, D. R. Klein, R. Cheng, K. L. Seyler, D. Zhong, E. Schmidgall, M. A. McGuire, D. H. Cobden, W. Yao, D. Xiao, P. Jarillo-Herrero, and X. Xu, Layer-dependent ferromagnetism in a van der waals crystal down to the monolayer limit, *Nature* **546**, 270 (2017).
- [2] C. Gong, L. Li, Z. Li, H. Ji, A. Stern, Y. Xia, T. Cao, W. Bao, C. Wang, Y. Wang, Z. Q. Qiu, R. J. Cava, S. G. Louie, J. Xia, and X. Zhang, Discovery of intrinsic ferromagnetism in two-dimensional van der waals crystals, *Nature* **546**, 265 (2017).
- [3] H. Yang, S. O. Valenzuela, M. Chshiev, S. Couet, B. Dieny, B. Dlubak, A. Fert, K. Garello, M. Jamet, D.-E. Jeong, K. Lee, T. Lee, M.-B. Martin, G. S. Kar, P. S  n  or, H.-J. Shin, and S. Roche, Two-dimensional materials prospects for non-volatile spintronic memories, *Nature* **606**, 663 (2022).
- [4] A. Fert, R. Ramesh, V. Garcia, F. Casanova, and M. Bibes, Electrical control of magnetism by electric field and current-induced torques, *Rev. Mod. Phys.* **96**, 015005 (2024).
- [5] Q.-C. Sun, T. Song, E. Anderson, A. Brunner, J. F  rster, T. Shalomayeva, T. Taniguchi, K. Watanabe, J. Gr  fe, R. St  hr, X. Xu, and J. Wrachtrup, Magnetic domains and domain wall pinning in atomically thin crbr3 revealed by nanoscale imaging, *Nature Communications* **12**, 1989 (2021).
- [6] H.-H. Yang, N. Bansal, P. R   mann, M. Hoffmann, L. Zhang, D. Go, Q. Li, A.-A. Haghighirad, K. Sen, S. Bl  gel, M. Le Tacon, Y. Mokrousov, and W. Wulfhekel, Magnetic domain walls of the van der waals material fe3gete2, *2D Materials* **9**, 025022 (2022).
- [7] D. Kumar, T. Jin, R. Sbiaa, M. Kl  ui, S. Bedanta, S. Fukami, D. Ravelosona, S.-H. Yang, X. Liu, and S. N. Piramanayagam, Domain wall memory: Physics, materials, and devices, *Physics Reports* **958**, 1 (2022).
- [8] N. D. Mermin and H. Wagner, Absence of ferromagnetism or antiferromagnetism in one- or two-dimensional isotropic heisenberg models, *Phys. Rev. Lett.* **17**, 1133 (1966).
- [9] R. Roemer, C. Liu, and K. Zou, Robust ferromagnetism in wafer-scale monolayer and multilayer fe3gete2, *npj 2D Materials and Applications* **4**, 33 (2020).
- [10] M. Bode, M. Heide, K. von Bergmann, P. Ferriani, S. Heinze, G. Bihlmayer, A. Kubetzka, O. Pietzsch, S. Bl  gel, and R. Wiesendanger, Chiral magnetic order at surfaces driven by inversion asymmetry, *Nature* **447**, 190 (2007).
- [11] S. Grytsiuk, M. Hoffmann, J.-P. Hanke, P. Mavropoulos, Y. Mokrousov, G. Bihlmayer, and S. Bl  gel, Ab initio analysis of magnetic properties of the prototype b20 chiral magnet fege, *Phys. Rev. B* **100**, 214406 (2019).
- [12] Y. Ga, Q. Cui, J. Liang, D. Yu, Y. Zhu, L. Wang, and H. Yang, Dzyaloshinskii-moriya interaction and magnetic skyrmions induced by curvature, *Phys. Rev. B* **106**, 054426 (2022).
- [13] H. B. Tran and Y. ichiro Matsushita, Skyrmions in van der waals centrosymmetric materials with dzyaloshinskii-moriya interactions, *Scripta Materialia* **239**, 115799 (2024).
- [14] K. Wang, V. Bheemarasetty, J. Duan, S. Zhou, and G. Xiao, Fundamental physics and applications of skyrmions: A review, *Journal of Magnetism and Magnetic Materials* **563**, 169905 (2022).
- [15] D. Amoroso, P. Barone, and S. Picozzi, Spontaneous skyrmionic lattice from anisotropic symmetric exchange in a ni-halide monolayer, *Nature Communications* **11**, 5784 (2020).
- [16] G. Mart  nez-Carracedo, L. Oroszl  ny, A. Garc  a-Fuente, B. Ny  ri, L. Udvardi, L. Szunyogh, and J. Ferrer, Relativistic magnetic interactions from nonorthogonal basis sets, *Phys. Rev. B* **108**, 214418 (2023).
- [17] H. J. Xiang, E. J. Kan, S.-H. Wei, M.-H. Whangbo, and X. G. Gong, Predicting the spin-lattice order of frustrated systems from first principles, *Phys. Rev. B* **84**, 224429 (2011).
- [18] M.-G. Han, J. D. Thomsen, J. P. Philbin, J. Mun, E. Park, F. Camino, L. D  kanovsk  y, C. Liu, Z. Sofer,



- P. Narang, F. M. Ross, and Y. Zhu, Electric-field control of magnetic skyrmion chirality in a centrosymmetric 2d van der waals magnet (2024), arXiv:2406.00785.
- [19] Y. Ren, Y. Ge, W. Wan, Q. Li, and Y. Liu, Two dimensional ferromagnetic semiconductor: monolayer crges<sub>3</sub>, *Journal of Physics: Condensed Matter* **32**, 015701 (2019).
- [20] K.-R. Hao, X.-Y. Ma, H.-Y. Lyu, Z.-G. Zhu, Q.-B. Yan, and G. Su, The atlas of ferroicity in two-dimensional mgex<sub>3</sub> family: Room-temperature ferromagnetic half metals and unexpected ferroelectricity and ferroelasticity, *Nano Research* **14**, 4732 (2021).
- [21] L. Chen, C. Mao, J.-H. Chung, M. B. Stone, A. I. Kolesnikov, X. Wang, N. Murai, B. Gao, O. Delaire, and P. Dai, Anisotropic magnon damping by zero-temperature quantum fluctuations in ferromagnetic crgete<sub>3</sub>, *Nature Communications* **13**, 4037 (2022).
- [22] F. Zhu, L. Zhang, X. Wang, F. J. dos Santos, J. Song, T. Mueller, K. Schmalzl, W. F. Schmidt, A. Ivanov, J. T. Park, J. Xu, J. Ma, S. Lounis, S. Blügel, Y. Mokrousov, Y. Su, and T. Brückel, Topological magnon insulators in two-dimensional van der waals ferromagnets crsite<sub>i</sub>sub<sub>j</sub>3<sub>i</sub>/sub<sub>j</sub> and crgete<sub>i</sub>sub<sub>j</sub>3<sub>i</sub>/sub<sub>j</sub>: Toward intrinsic gap-tunability, *Science Advances* **7**, eabi7532 (2021), <https://www.science.org/doi/pdf/10.1126/sciadv.abi7532>.
- [23] Y. F. Li, W. Wang, W. Guo, C. Y. Gu, H. Y. Sun, L. He, J. Zhou, Z. B. Gu, Y. F. Nie, and X. Q. Pan, Electronic structure of ferromagnetic semiconductor crgete<sub>3</sub> by angle-resolved photoemission spectroscopy, *Phys. Rev. B* **98**, 125127 (2018).
- [24] Y. Zhang, C. Xu, P. Chen, Y. Nahas, S. Prokhorenko, and L. Bellaiche, Emergence of skyrmionium in a two-dimensional crge(se, te)<sub>3</sub> janus monolayer, *Phys. Rev. B* **102**, 241107 (2020).
- [25] Z. Sun, X. Li, J. Li, Y. Wei, H. Guo, and J. Wang, Intrinsic bitunable magnetism/polarity behavior in 2d janus cr2i3y3 (y = f, cl, or br) systems, *npj 2D Materials and Applications* **6**, 69 (2022).
- [26] C. Xu, J. Feng, S. Prokhorenko, Y. Nahas, H. Xiang, and L. Bellaiche, Topological spin texture in janus monolayers of the chromium trihalides cr(i, X)<sub>3</sub>, *Phys. Rev. B* **101**, 060404 (2020).
- [27] T. Gorkan, J. Das, J. Kapeghian, M. Akram, J. V. Barth, S. Tongay, E. Akturk, O. Erten, and A. S. Botana, Skyrmion formation in ni-based janus dihalide monolayers: Interplay between magnetic frustration and dzyaloshinskii-moriya interaction, *Phys. Rev. Mater.* **7**, 054006 (2023).
- [28] Y. Hou, F. Xue, L. Qiu, Z. Wang, and R. Wu, Multifunctional two-dimensional van der waals janus magnet cr-based dichalcogenide halides, *npj Computational Materials* **8**, 120 (2022).
- [29] G. Martínez-Carracedo, L. Oroszlány, A. García-Fuente, L. Szunyogh, and J. Ferrer, Electrically driven singlet-triplet transition in triangulene spin-1 chains, *Phys. Rev. B* **107**, 035432 (2023).
- [30] R. Xu and X. Zou, Electric field-modulated magnetic phase transition in van der waals cri<sub>3</sub> bilayers, *The Journal of Physical Chemistry Letters* **11**, 3152 (2020).
- [31] S. J. Callori, S. Hu, J. Bertinshaw, Z. J. Yue, S. Danilkin, X. L. Wang, V. Nagarajan, F. Klöse, J. Seidel, and C. Ulrich, Strain-induced magnetic phase transition in srcoo<sub>3-δ</sub> thin films, *Phys. Rev. B* **91**, 140405 (2015).
- [32] J. Cenker, S. Sivakumar, K. Xie, A. Miller, P. Thijssen, Z. Liu, A. Dismukes, J. Fonseca, E. Anderson, X. Zhu, X. Roy, D. Xiao, J.-H. Chu, T. Cao, and X. Xu, Reversible strain-induced magnetic phase transition in a van der waals magnet, *Nature Nanotechnology* **17**, 256 (2022).
- [33] Y. Sun, T. Lin, N. Lei, X. Chen, W. Kang, Z. Zhao, D. Wei, C. Chen, S. Pang, L. Hu, L. Yang, E. Dong, L. Zhao, L. Liu, Z. Yuan, A. Ullrich, C. H. Back, J. Zhang, D. Pan, J. Zhao, M. Feng, A. Fert, and W. Zhao, Experimental demonstration of a skyrmion-enhanced strain-mediated physical reservoir computing system, *Nature Communications* **14**, 3434 (2023).
- [34] R. Kumar, C. Fillion, B. Lovery, I. Benguetat-El Mokhtari, I. Joumard, S. Auffret, L. Ranno, Y. Rousigné, S. Chérif, A. Stashkevich, M. Belmeguenai, C. Baraduc, and H. Béa, Control of skyrmion chirality in Ta/Fe-Co-B/tao<sub>x</sub> trilayers by tao<sub>x</sub> oxidation and Fe-Co-B thickness, *Phys. Rev. Appl.* **19**, 024064 (2023).
- [35] M. Šiškins, S. Kurdi, M. Lee, B. J. M. Slotboom, W. Xing, S. Mañas-Valero, E. Coronado, S. Jia, W. Han, T. van der Sar, H. S. J. van der Zant, and P. G. Steeneken, Nanomechanical probing and strain tuning of the curie temperature in suspended cr2ge2te6-based heterostructures, *npj 2D Materials and Applications* **6**, 41 (2022).
- [36] P. Hohenberg and W. Kohn, Inhomogeneous electron gas, *Physical Review* **136**, B864 (1964).
- [37] W. Kohn and L. J. Sham, Self-consistent equations including exchange and correlation effects, *Physical Review* **140**, A1133 (1965).
- [38] J. M. Soler, E. Artacho, J. D. Gale, A. García, J. Junquera, P. Ordejón, and D. Sánchez-Portal, The siesta method for ab initio order-n materials simulation, *Journal of Physics: Condensed Matter* **14**, 2745 (2002).
- [39] A. Liechtenstein, M. Katsnelson, V. Antropov, and V. Gubanov, Local spin density functional approach to the theory of exchange interactions in ferromagnetic metals and alloys, *J. Magn. Magn. Mater.* **67**, 65 (1987).
- [40] L. Udvardi, L. Szunyogh, K. Palotás, and P. Weinberger, First-principles relativistic study of spin waves in thin magnetic films, *Phys. Rev. B* **68**, 104436 (2003).
- [41] J. P. Perdew, K. Burke, and M. Ernzerhof, Generalized gradient approximation made simple, *Phys. Rev. Lett.* **77**, 3865 (1996).
- [42] N. Troullier and J. L. Martins, Efficient pseudopotentials for plane-wave calculations, *Phys. Rev. B* **43**, 1993 (1991).
- [43] P. Rivero, V. Manuel García-Suárez, D. Pereñiguez, K. Utt, Y. Yang, L. Bellaiche, K. Park, J. Ferrer, and S. Barraza-Lopez, Systematic pseudopotentials from reference eigenvalue sets for dft calculations: Pseudopotential files, *Data in Brief* **3**, 21 (2015).
- [44] J. B. Goodenough, Theory of the role of covalence in the perovskite-type manganites [La, m(II)]Mno<sub>3</sub>, *Phys. Rev.* **100**, 564 (1955).
- [45] J. Kanamori, Superexchange interaction and symmetry properties of electron orbitals, *Journal of Physics and Chemistry of Solids* **10**, 87 (1959).
- [46] P. W. Anderson, New approach to the theory of superexchange interactions, *Phys. Rev.* **115**, 2 (1959).
- [47] A. Otero Fumega, J. Phillips, and V. Pardo, Controlled two-dimensional ferromagnetism in 1t-crte<sub>2</sub>: The role of charge density wave and strain, *The Journal of Physical Chemistry C* **124**, 21047 (2020).
- [48] X. Chen, J. Qi, and D. Shi, Strain-engineering of magnetic coupling in two-dimensional magnetic semiconduc-

- tor crsite3: Competition of direct exchange interaction and superexchange interaction, *Physics Letters A* **379**, 60 (2015).
- [49] R. Xiao, Z. Guan, D. Feng, and C. Song, Strain-tunable ferromagnetism and skyrmions in two-dimensional Janus Cr<sub>2</sub>XYTe<sub>6</sub> (X, Y = Si, Ge, Sn, and X≠Y) monolayers, *Journal of Applied Physics* **135**, 043901 (2024).
- [50] J. Pang, X. Niu, M. Zhang, Y. Tang, Y. Zhang, and L. Bellaiche, Electric-field-induced formation and annihilation of skyrmions in a two-dimensional magnet, *Phys. Rev. B* **108**, 134430 (2023).
- [51] J. Liu, M. Shi, J. Lu, and M. P. Anantram, Analysis of electrical-field-dependent dzyaloshinskii-moriya interaction and magnetocrystalline anisotropy in a two-dimensional ferromagnetic monolayer, *Phys. Rev. B* **97**, 054416 (2018).
- [52] H. Yang, O. Boule, V. Cros, A. Fert, and M. Chshiev, Controlling dzyaloshinskii-moriya interaction via chirality dependent atomic-layer stacking, insulator capping and electric field, *Scientific Reports* **8**, 12356 (2018).
- [53] T. Koyama, Y. Nakatani, J. Ieda, and D. Chiba, Electric field control of magnetic domain wall motion via modulation of the dzyaloshinskii-moriya interaction, *Science Advances* **4**, eaav0265 (2018), <https://www.science.org/doi/pdf/10.1126/sciadv.aav0265>.
- [54] K. Pang, X. Xu, R. Ku, Y. Wei, T. Ying, W. Li, J. Yang, X. Li, and Y. Jiang, Ferroelectricity and high curie temperature in a 2d janus magnet, *ACS Applied Materials & Interfaces* **15**, 10133 (2023).
- [55] Q. Cui, Y. Zhu, J. Jiang, J. Liang, D. Yu, P. Cui, and H. Yang, Ferroelectrically controlled topological magnetic phase in a janus-magnet-based multiferroic heterostructure, *Phys. Rev. Res.* **3**, 043011 (2021).
- [56] A. Mahajan and S. Bhowmick, Magnetolectric multiferroic janus monolayers voxy (x/y = f, cl, br, or i, and x ≠ y) with in-plane ferroelectricity and out-of-plane piezoelectricity, *The Journal of Physical Chemistry C* **127**, 11407 (2023).
- [57] D. Bennett, Theory of polar domains in moiré heterostructures, *Phys. Rev. B* **105**, 235445 (2022).
- [58] D. Bennett, G. Martínez-Carracedo, X. He, J. Ferrer, P. Ghosez, R. Comin, and E. Kaxiras, Stacking-engineered ferroelectricity and multiferroic order in van der waals magnets (2024), arXiv:2405.20069 [cond-mat.mtrl-sci].
- [59] H. Jia, B. Zimmermann, G. Michalicek, G. Bihlmayer, and S. Blügel, Electric dipole moment as descriptor for interfacial dzyaloshinskii-moriya interaction, *Phys. Rev. Mater.* **4**, 024405 (2020).
- [60] J. Spethmann, M. Grünebohm, R. Wiesendanger, K. von Bergmann, and A. Kubetzka, Discovery and characterization of a new type of domain wall in a row-wise antiferromagnet, *Nature Communications* **12** (2021).
- [61] H. J. Elmers, S. Haldar, K. Medjanik, S. Babenkov, O. Fedchenko, D. Vasilyev, S. Heinze, and G. Schönhense, Critical behavior and exchange splitting in the two-dimensional antiferromagnet mn on re(0001), *Phys. Rev. B* **107**, 144424 (2023).
- [62] T. Moriya, Anisotropic superexchange interaction and weak ferromagnetism, *Phys. Rev.* **120**, 91 (1960).